Materials Science-Poland, 34(3), 2016, pp. 503-516
http://www.materialsscience.pwr.wroc.pl/
DOI: 10.1515/msp-2016-0078

DE GRUYTER OPEN

Anisotropic elastic properties of Fe_xB (x = 1, 2, 3) under pressure. First-principles study

A. GUEDDOUH[1,2*], B. BENTRIA[1], Y. BOUROUROU[3], S. MAABED[1]

[1]Laboratoire de Physique des Matériaux, Université Amar Telidji de Laghouat; BP37G, Laghouat 03000, Algeria
[2]Département de Physique, Faculté des Sciences, Université A.B. Belkaid Tlemcen, BP 119, Tlemcen 13000, Algeria
[3]Laboratory University of Sidi Bel-Abbčs, 22000 Sidi Bel-Abbčs, Algeria

Spin-polarization (SP) and pressure effects have been used to better clarify and understand anisotropic elastic properties of Fe–B intermetallic compounds using the first-principles calculation with generalized gradient approximation (GGA) within the plane-wave pseudopotential density functional theory. Elastic properties, including bulk, shear and Young's moduli as well as Poisson ratio were obtained by Voigt-Reuss-Hill approximation. All studied Fe–B compounds were mechanically stable. The brittle and ductile properties were discussed using bulk to shear moduli ratio (B/G) of the studied structures in the pressure range of 0 GPa to 90 GPa in order to predict the critical pressure of phase transition from ferromagnetic (FM) to nonmagnetic (NM) state. Mechanical anisotropy in both cases was discussed by calculating different anisotropic indexes and factors. We have plotted three-dimensional (3D) surfaces and planar contours of the bulk and Young's moduli of Fe_xB (x = 1, 2, 3) compounds for some crystallographic planes, (1 0 0), (0 1 0) and (0 0 1), to reveal their elastic anisotropy. On the basis of anisotropic elastic properties the easy and hard axes of magnetization for the three studied compounds were predicted.

Keywords: *DFT; spin polarization; elastic properties; anisotropy; easy and hard axes*

1. Introduction

In the past decades, the binary Fe–B alloy system has been a subject of numerous experimental and theoretical studies concerning hardness, melting point, wear resistance, corrosion resistance, and ferromagnetism [1–3]. According to the Fe–B equilibrium phase diagram, there are two stable iron borides at ambient temperature: single boride layer (Fe_2B) or double (FeB and Fe_2B) layers [4]. The metastable phase, Fe_3B, appears during formation of Fe_2B. The metastable o-Fe_3B phase has also been obtained in Fe–B glasses by quenching and annealing [5]. These compounds can be prepared using numerous equilibrium or non-equilibrium methods, such as ball milling, chemical vapor deposition (CVD), physical vapor deposition (PVD), magnetic sputtering and thermal chemical reactions. Fe_2B can also be prepared as a bulk single crystal [6]. FeB was prepared in a form of nanoparticles by chemical reduction method [7] in order to improve the cycle stability of $PuNi_3$-type hydrogen storage electrodes [8, 9]. The properties depending on process time and temperature, such as structure parameters, hardness, Young's modulus and fracture toughness of iron boride layers have been investigated experimentally [10]. The electronic structure, stability and elastic constants of the three Fe_xB compounds were calculated in the literature [11] using DFT. It was indicated that pressure affects the structure, mechanical and magnetic properties of iron borides, and spin-polarized calculations were important to obtain the correct ground state properties of Fe_xB compounds. We tried to demonstrate that the structure properties and magnetic moment change strongly with pressure.

In this work, we performed the first principles calculations of anisotropic elastic properties for the three structures Fe_xB (x = 1, 2, 3) at 0 GPa pressure and at a critical pressure when a ferromagnetic material undergoes transition to a nonmagnetic state

*E-mail: ghahmed2012@gmail.com

(NM). Anisotropy index A and directional dependences of bulk and Young's moduli were investigated. From the anisotropic elastic properties, the easy and hard axes of magnetization of the three compounds were predicted, which revealed that for bcc Fe the highest density of atoms is in the ⟨1 1 1⟩ direction, and consequently ⟨1 1 1⟩ is the hard magnetization axis. In contrast, the atom density is the lowest in ⟨1 0 0⟩ direction, and consequently ⟨1 0 0⟩ is the easy magnetization axis. Certainly, since bcc iron is a cubic crystal, all six cube edge orientations ⟨1 0 0⟩, ⟨0 1 0⟩, ⟨0 0 1⟩, ⟨$\bar{1}$ 0 0⟩, ⟨0 $\bar{1}$ 0⟩ and ⟨0 0 $\bar{1}$⟩ are in fact equivalent easy axes [12].

We hope that our study will provide a useful guidance for future works on the Fe–B compounds.

Finally, we concluded that spin-polarization and pressure are of significant importance in determining the anisotropic elastic properties of iron borides.

2. Structure aspects and calculation methods

FeB and Fe_3B belong to an orthorhombic space group Pnma (Fig. 1) [13–16]. Both structures contain four formula units per cell. In Fe_3B, the isotype of Fe_3C, iron atoms are distributed over two distinct lattice sites: the general Fe sites (Wyckoff position 8d) and the special Fe sites (Wyckoff position 4c). In contrast, Fe_2B (Fig. 1) belongs to the body-centered tetragonal Bravais lattice with I4/mcm space group where the unit cell contains four equivalent Fe atoms in the positions of point group mm and two equivalent B atoms in the positions of point group 42 [11]. The B atoms in Fe_2B are located between two layers of Fe atoms in a distorted, closely packed arrangement.

Total energy calculations were performed within the density functional theory (DFT) [17]. CASTEP code was used in this study. The last uses the plane wave in reciprocal space [18]. The ultrasoft Vanderbilt pseudopotentials were employed to represent the electrostatic interactions between valence electrons and ionic cores [19]. They were used with the following valence electronic configurations Fe: $3d^6 4s^2$ and B: $2s^2 2p^1$. Generalized gradient approximation PBE-GGA was used for exchange-correlation energy calculations [20]. The kinetic energy cut-off value was selected as 500 eV, which was sufficient to obtain reliable results.

Total energies were evaluated in the first irreducible Brillouin zone with the following Monkhorst-pack grids [21]: (6 × 10 × 8) for FeB, (10 × 10 × 10) for Fe_2B and (10 × 12 × 8) for Fe_3B. It is known that the ground states of several Fe_xB compounds are ferromagnetic [22].

Structural and elastic properties were calculated for both FM and NM states in the three compounds. The convergence criteria of total energy and structure optimization were set to fine quality with the energy tolerance of 10^{-6} eV/atom. BFGS (Broydene-Fletchere-Goldarbe-Shanno) optimization method was used to obtain the equilibrium crystal structures of Fe_xB with maximum atom displacement and force set to 0.002 Å and 0.001 eV/Å.

The cohesive energy (E_{coh}) of a material, (which is a useful fundamental property), is a measure of the relative binding forces. The stability of our compounds was evaluated by calculating two energy parameters, cohesive energy E_{coh} and formation energy E_f defined as:

$$E_{coh}(Fe_xB) = \frac{E_{total}(Fe_xB, Cell) - xnE_{iso}(Fe) - nE_{iso}(B)}{n} \quad (1)$$

$$E_f(Fe_xB) = E_{coh}(Fe_xB) - xE_{coh}(Fe) - E_{coh}(B) \quad (2)$$

where E_{coh} (Fe_xB) is the cohesive energy of Fe_xB per unit formula; E_f (Fe_xB) is its formation energy; E_{coh} (Fe) is the cohesive energy of iron element per atom; E_{total} (Fe_xB, Cell) is the total calculated energy of Fe_xB per conventional unit cell; E_{iso}(Fe) is the total energy of an isolated Fe atom and finally n refers to the number of unit formula Fe_xB in the conventional cell. The calculation method for E_{coh} (Fe_xB) can also be used to evaluate the cohesive energy of pure elements B and Fe. Equation 1 and equation 2 require negative values of E_{coh} (Fe_xB) and E_f (Fe_xB) to refer to a thermodynamically stable structure. The crystal structures of Fe_xB

studied in this paper were built based on experimental results.

3. Results and discussion

3.1. Structural properties and stability

The calculated lattice parameters, unit cell volume, bulk modulus, cohesive energy and the formation energy for Fe_xB along with the available experimental and previous theoretical data for comparison have been discussed by Gueddouh et al. [11]. The results show that the calculated structure parameters are in good agreement with the experimental values. The calculated values of cohesive energies of FeB, Fe_2B and Fe_3B indicate that all of the Fe_xB compounds are stable. Furthermore, the cohesive energies decrease from FeB to Fe_3B, which is mainly caused by the increase in the volume concentration of Fe atoms.

3.2. Pressure effects

In order to induce a significant change in a structure, high pressure is usually needed to study the material. By increasing the pressure, a transfer from magnetic to nonmagnetic state occurs, which causes an extinction of the magnetic moment; the critical (transition) pressure was estimated as 77 GPa, 85 GPa and 55 GPa for FeB, Fe_2B and Fe_3B, respectively, as shown in Fig. 2. Usually, the critical pressure at which a ferromagnetic material undergoes transition to a NM state is defined as $Pc = -\Delta E/\Delta V$ where ΔE is the difference between NM and spin-polarized (SP) equilibrium total energy by unit cell and ΔV is the respective difference between NM and SP equilibrium volumes. This definition of critical pressure (P_c) was first employed by Mohn et al. [23, 24] in their work on magneto-elastic anomalies in Fe–Ni Invar alloys [23] and $NiFe_3N$ and $PdFe_3N$ nitrides [24]. This definition is also used in the study on magnetic transition of intermetallic bilayers and substituted iron nitrides [25].

The calculated percentage change of volume at 0 GPa and at transition pressure for our three compounds [11] showed a volume compression of 15 %, 20 % and 19 % for FeB, Fe_2B and Fe_3B, respectively, at the applied pressure, which resulted in an increase in the bulk modulus of our compounds by 47.7 %, 62 % and 61.8 %.

The formation energy E_f was calculated to check the probability of thermodynamic existence of Fe_xB under pressure. All formation energies are negative indicating that all the structures in the two pressure conditions are thermodynamically stable. The formation energies of Fe_xB in magnetic state are less than those of Fe_xB in NM state by 4.7 %, 3.9 %, 7.1 %, implying that Fe_xB(FM) has better thermodynamic stability.

The calculated magnetic moments of our compounds at 0 GPa are in good agreement with theoretical and experimental values [26] and are 2.003 μB, 1.83 μB and 1.12 μB for Fe_3B, Fe_2B and FeB, respectively, which results from the difference between the density of spin-up and spin-down electrons and corresponds to the saturated magnetic moment, μ_{sat}, at T = 0, as shown Fig. 3. It appears that Fe_3B has the highest magnetic moment which leads to a shift in the Slater-Pauling curve [27]. These moments are smaller than the magnetic moments of pure bcc ferromagnetic iron which behaves as a weak ferromagnetic with a magnetic moment of 2.217 μB [28]. Indeed, when B atoms are inserted in Fe crystal, the volume concentration of metallic Fe–Fe bonds decreases and they are replaced by the newly formed covalent Fe–B and B–B.

The magnitude of the magnetic moment is strongly related to the volume. Thus, the values of equilibrium volume obtained in the magnetic state are larger than in NM state. A possible origin of this dependence is a magneto-volume effect [29]. Because the Pauli Exclusion Principle operates for parallel spins, the electron kinetic energy in the spin-polarized state is higher, and volume expansion relaxes the kinetic energy. Consequently, the magnetic (high-spin) state has a larger volume than the non-magnetic state [30]. However, the bulk modulus decreases from FeB to Fe_3B. Also due to the pressure effect, the bulk modulus has increased from 0 % to 47.7 % for FeB, from 0 % to 62 % for Fe_2B and from 0 % to 61.8 % for Fe_3B. In the NM state the bulk modulus B is in general larger

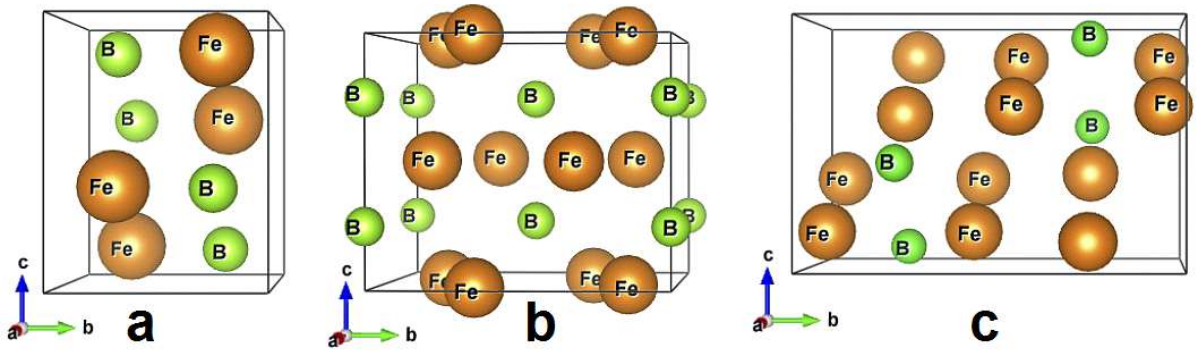

Fig. 1. Fe_xB structures: (a) FeB, (b) Fe_2B and (c) Fe_3B.

than in the magnetic state. The low value of bulk modulus in the magnetic state points out to a larger compressibility. This means that the system is "softer" when it is magnetically ordered and "harder" when it is not. The spin-polarization calculations are important to obtain the correct ground state properties of Fe_xB ferromagnetic compounds. The calculated magnetic moment as a function of pressure is presented in Fig. 2. Total DOS at the Fermi level for Fe_xB increases under pressure by 21 %, 50 % and 32.5 % for FeB, Fe_2B and Fe_3B, respectively (Fig. 3). This enhanced N (E_f) is derived entirely from the Fe 3d states, with negligible contribution from the B 2p states. Following the above arguments we may predict that the appearance of superconductivity in Fe_xB under pressure is similar to the case of iron that undergoes a transition to superconducting phase above 30 GPa when it loses its magnetic moment [31]. It is easy to observe that the magnetic moment decreases with increasing pressure.

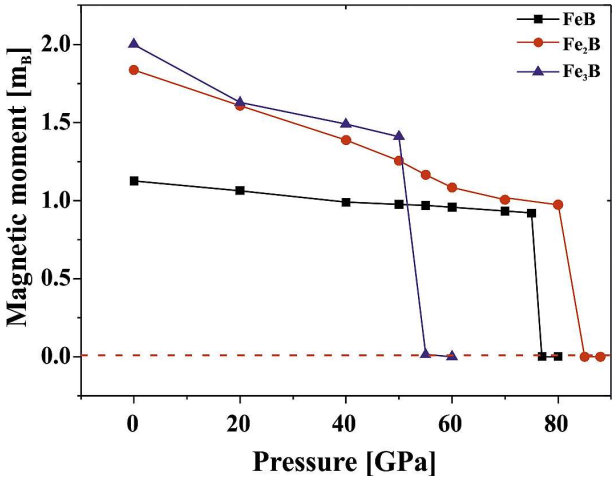

Fig. 2. Dependence of magnetic moment vs. pressure for Fe_xB [11].

4. Elastic properties under pressure

It is well known that elastic properties reflect interatomic interactions and are related to some fundamental physical properties, such as thermal expansion, phonon spectra and equations of state [32]. The elastic constants of single crystalline Fe_xB compounds are presented in Table 1. Generally, the elastic constants C_{11}, C_{22} and C_{33} are very high, both at zero and critical pressure, which indicates high resistance to the axial compression in these directions. However, the magnitude orders in three axes are different. For orthorhombic FeB and Fe_3B, the order is $C_{33} > C_{22} > C_{11}$. For tetragonal Fe_2B the order is $C_{11} > C_{33}$. Since the tetragonal structure can be regarded as a special case of orthorhombic structure with an additional condition of a = b, the mechanical stability criteria can be represented in a uniform manner for orthorhombic structure [33]:

$$C_{ii} > 0 \; (i = 1;2;3;4;5;6) \qquad (3)$$

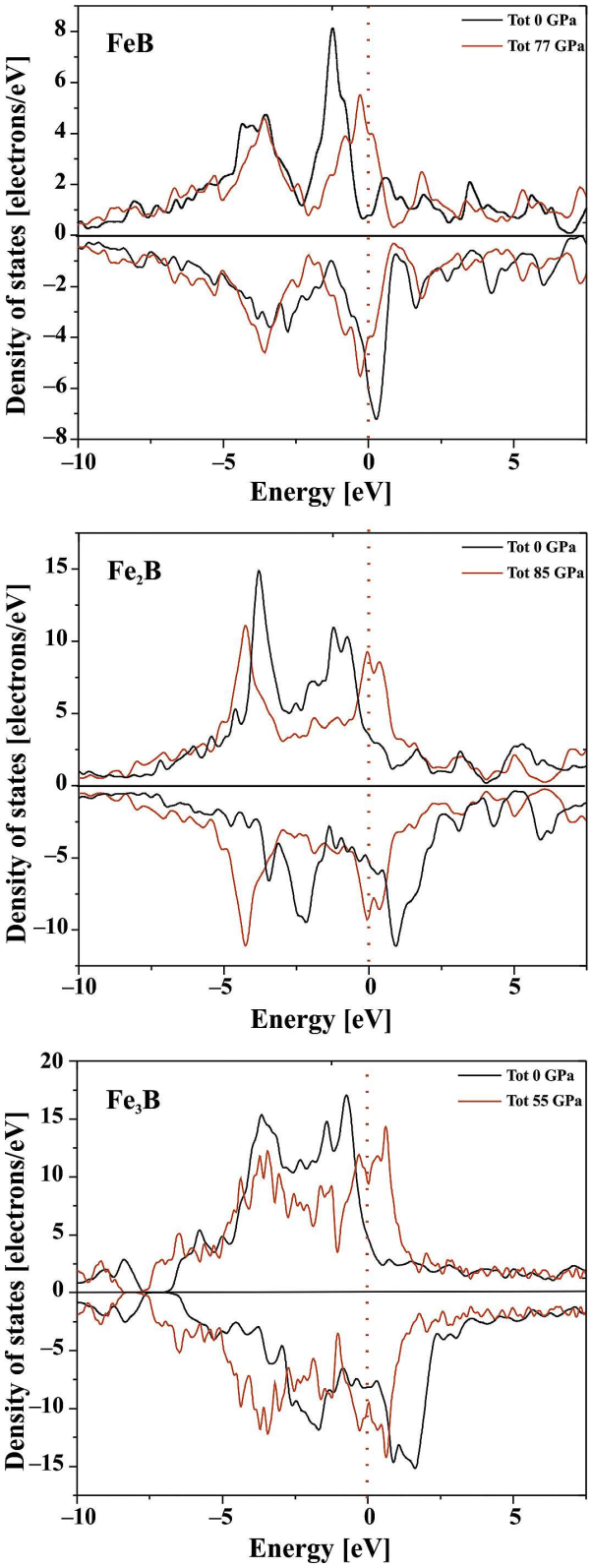

Fig. 3. The calculated total DOS with spin polarization and at critical pressure of Fe_xB.

$$C_{11}+C_{22}+C_{33}+2(C_{12}+C_{13}+C_{23})>0,$$
$$(C_{11}+C_{22}-2C_{12})>0;(C_{11}+C_{33}-2C_{13})>0 \quad (4)$$

$$(C_{22}+C_{33}-2C_{23})>0 \quad (5)$$

On the other hand, the mechanical stability leads to restrictions on the elastic coefficients under isotropic pressure as follows:

$$\tilde{C_{ii}}=C_{ii}-P>0,\ (i=1,2,3,4,5,6) \quad (6)$$

$$(C_{11}+C_{22}-2C_{12}-4P)>0 \quad (7)$$

For tetragonal structure the elastic constants under pressure P are related to those under zero pressure, as follows [34]:

$$\tilde{C_{ij}}=C_{ij}(i=1,2,3;j=4,5,6) \quad (8)$$

$$\tilde{C_{ii}}=C_{ii}-P(i=1,2,3,4,5,6) \quad (9)$$

$$\tilde{C_{12}}=C_{12}+P \quad (10)$$

$$\tilde{C_{13}}=C_{13}+P,$$
$$\tilde{C_{23}}=C_{23}+P,$$
$$\tilde{C_{45}}=C_{45},$$
$$\tilde{C_{46}}=C_{46} \quad (11)$$

$$\tilde{C_{56}}=C_{56} \quad (12)$$

The stability criteria of material under pressure are similar to those under zero pressure, just replacing C_{ij} with $\tilde{C}_{ij}$ (i = j = 1, 2, 3, 4, 5, 6) [35]. As for Fe_2B in the tetragonal structure, there are six independent elastic constants, C_{11}, C_{12}, C_{13}, C_{33}, C_{44}, C_{66}, because $C_{22}=C_{11}$, $C_{23}=C_{13}$, $C_{44}=C_{55}$ as a result of the crystal symmetry. The single crystal elastic coefficients (C_{ij}) satisfy the stability criteria, which leads to the following restrictions on the elastic coefficients under isotropic pressure:

$$\tilde{C_{ii}}>0,\ (i=1,2,3,\ldots 6),\tilde{C_{11}}+\tilde{C_{33}}-2\tilde{C_{13}}>0 \quad (13)$$

$$2\tilde{C_{11}}+\tilde{C_{33}}+2\tilde{C_{12}}+4\tilde{C_{13}}>0 \quad (14)$$

$$(\tilde{C_{11}}-\tilde{C_{12}})>0 \quad (15)$$

C_{ij} are the elements of elastic coefficient matrix. The arithmetic average of the Voigt and Reuss bounds is known as the Voigt-Reuss-Hill (VRH) average, which is regarded as the best estimate for the theoretical value of polycrystalline elastic modulus [11]:

$$G_H = (G_R + G_V)/2 \tag{16}$$

$$B_H = (B_R B_V)/2 \tag{17}$$

The Young's modulus and Poisson ratio can be computed from the formula [11]:

$$E = 9BG/(3B + G) \tag{18}$$

$$\nu = (3B - 2G)/(6B + 2G) \tag{19}$$

A larger B/G value (>1.75) for a solid indicates ductile behavior while a smaller B/G value (<1.75) usually means brittle material [36]. Similarly, Poisson ratio $\nu > 0.26$ relates to ductile compounds usually [36]. At both pressures studied here 0 GPa and the critical pressure, B/G > 1.75 and $\nu > 0.26$ is larger than 0.26 for FeB and Fe_3B (Table 3), which indicates that FeB and Fe_3B are ductile. The values of B/G and ν for Fe_2B are 1.52 and 0.23, respectively, at 0 GPa pressure which means that Fe_2B is brittle. In contrast, at critical pressure Fe_2B is ductile (B/G = 2.48, $\nu = 0.32$).

5. Elastic anisotropy

It is known that elastic anisotropy correlates with anisotropic plastic deformation and behavior of microcracks in material. Hence, it is important to study elastic anisotropy in intermetallics structures in order to further understand these properties and improve their mechanical durability. Most of crystals exhibit elastic anisotropy to some extent, and several criteria have been developed to describe it. The elastic anisotropy of a crystal can be characterized by the universal anisotropic index A^U and by the indexes describing the behavior in shear and compression (A_G and A_B). The universal elastic anisotropy index A^U and indexes A_G and A_B for a crystal with any symmetry may be proposed as follows [37, 38]:

$$A^U = 5\frac{G_V}{G_R} + \frac{B_V}{B_R} - 6 \leqslant 0 \tag{20}$$

$$A_G = \frac{G_V - G_R}{G_V + G_R} \times 100 \tag{21}$$

$$A_B = \frac{B_V - B_R}{B_V + B_R} \times 100 \tag{22}$$

where B_V (G_V) and B_R (G_R) are the bulk modulus (shear modulus) in the Voigt and Reuss approximations respectively. $A^U = 0$ corresponds to the isotropy of the crystal. The deviation of A^U from zero defines the extent of single crystal anisotropy and accounts for both shear and bulk contribution, unlike all other existing anisotropy measures. Thus, A^U represents a universal measure to quantify a single crystal elastic anisotropy. $A_B = A_G = 0$ represents the elastic isotropic crystal, while $A_B = A_G = 1$ means the maximum elastic anisotropy [39]. From Table 2, it can be seen that the mechanical anisotropy of FeB is stronger than in other structures. In Fig. 5, we have outlined the projections of Young's modulus in (0 0 1), (0 1 0) and (1 0 0) crystal planes. We can clearly show that the anisotropy of FeB is stronger than in Fe_2B and Fe_3B in the three planes. The results are also in good agreement with the calculated anisotropic indexes in Table 2.

The shear anisotropic factors provide a measure of the degree of anisotropy in atomic bonding in different crystallographic planes. The shear anisotropic factor for an orthorhombic crystal can be measured by three factors (Zener ratios) [40–42]:

1. The shear anisotropic factor for the $\{1\ 0\ 0\}$ shear planes between $\langle 0\ 1\ 1\rangle$ and $\langle 0\ 1\ 0\rangle$ directions is defined as:
2. The anisotropic factor for the $\{0\ 1\ 0\}$ shear planes between $\langle 1\ 0\ 1\rangle$ and $\langle 0\ 0\ 1\rangle$ directions is:

$$A_2 = \frac{4C_{55}}{C_{22} + C_{33} - 2C_{23}} \tag{23}$$

and

Table 1. The calculated full set of elastic constants of Fe_xB (GPa) [11].

Species	Elastic constants								
	C_{11}	C_{22}	C_{33}	C_{12}	C_{13}	C_{23}	C_{44}	C_{55}	C_{66}
FeB (0 GPa)	389.82	438.36	557.07	286.85	183.12	239.76	218.8	132.25	212.01
	373.7[a]	434.1[a]	503.4[a]	246[a]	184.4[a]	209.1[a]	207.4[a]	117.7[a]	193.7[a]
FeB (77 GPa)	718.5	752.6	993.9	583.2	350.1	492.4	296.4	243.3	354.4
Fe_2B	459.7		426.3	165.6	132.3		162.6		173.7
(0 GPa)	413[b]		389[b]	154[b]	132[b]		148[b]		157[b]
Fe_2B (85 GPa)	1010.4		839	541.3	488.4		298		288.4
Fe_3B (0 GPa)	281.7	337.5	354	126.7	165.3	182.2	130.2	118.7	175.6
	263.3[a]	302.7[a]	318.4[a]	133.5[a]	162.8[a]	178.6[a]	110.2[a]	101.2[a]	158.7[a]
Fe_3B (55 GPa)	694	826	778.5	485.5	444.75	403.6	193.1	195.8	307.7

[a][46], [b][47]

Table 2. Polycrystalline elastic properties and anisotropy factors of Fe-B system.

Species	B_V	B_R	G_V	G_R	A_1	A_2	A_3	A_u	A_G	A_B
FeB (0 GPa)	308.37	302.80	155.66	125.47	1.57	1.04	3.38	1.22	10.74	0.91
	287.8[a]	284.6[a]	148.5[a]	130.9[a]	1.63[a]	0.91[a]	2.45[a]	0.68[a]	5.85[a]	0.62[a]
FeB (77 GPa)	621.69	612.49	260.17	190.38	1.17	1.28	4.65	1.85	15.49	0.75
Fe_2B (0 GPa)	245.11	244.07	160.82	160.21	1.18	1.18	0.26	0.02	0.19	0.21
	222.7[a]	221.8[a]	144.4[a]	143.6[a]	1.07[a]	1.07[a]	1.23[a]	0.03[a]	0.28[a]	0.20[a]
Fe_2B (85 GPa)	655.09	646.32	266.31	260.30	1.23	1.23	0.34	0.13	1.14	0.67
Fe_3B (0 GPa)	213.51	207.55	118.15	107.50	1.71	1.45	1.92	0.52	4.72	1.41
	203.8[a]	199.5[a]	101.3[a]	90.6[a]	1.72[a]	1.53[a]	2.12[a]	0.61[a]	5.58[a]	1.07[a]
Fe_3B (55 GPa)	551.81	550.01	203.62	186.77	1.33	0.98	2.24	0.45	4.31	0.16

[a][46]

Table 3. The calculated bulk, Young's (E) and shear modulus (G) of Fe_xB (under 0 and critical pressure, in GPa), Poisson's ratio (v) and B/G ratio along with other available values.

Species	B	E	G	v	B/G
FeB (0 GPa)	305.6	365.7	140.6	0.30	2.174
	286.6[a]	360.5[a]	139.7[a]	0.29[a]	2.05[a]
FeB (77 GPa)	617.1	567.5	225.3	0.34	2.76
Fe_2B (0 GPa)	244.6	395.2	160.5	0.23	1.52
	222.3[a]	355[a]	144[a]	0.23[a]	1.54[a]
Fe_2B (85 GPa)	651	695.4	263	0.32	2.48
Fe_3B (0 GPa)	210	285.3	112	0.27	1.875
	201.6[a]	248.5[a]	96[a]	0.3[a]	2.1[a]
Fe_3B (55 GPa)	551	524	195.2	0.34	2.82

[a][46]

3. The anisotropic factor for the {0 0 1} shear planes between ⟨1 1 0⟩ and ⟨0 1 0⟩ directions is:

$$A_3 = \frac{4C_{66}}{C_{11} + C_{22} - 2C_{12}} \tag{24}$$

The calculated values of anisotropic factors for iron borides are shown in Table 2. For an isotropic crystal, all three factors must be one, while any value smaller or greater than one is a measure of degree of elastic anisotropy possessed by the crystal. Our results thus indicate a very large shear anisotropy on the (1 0 0) and (0 0 1) planes of FeB and Fe_3B due to the anomalously high C_{44} and C_{66} relatively to C_{55}. Thus, for Fe_2B the large shear anisotropy is on the (0 0 1) plane due to high C_{44} compared to C_{66}.

Taking also into account the strength characteristics of the studied compounds, which have low values of G/B ratio (0.46 for FeB, 0.66 for Fe_2B and 0.53 for Fe_3B), the ductility of the iron borides is a very important advantage and therefore they are intrinsically brittle.

The spin polarization and pressure increase the anisotropic factors A_1 by 25 % and 22 % for FeB and Fe_3B, respectively, and A_2 by 32 % for Fe_3B, but reduce the anisotropic factors A_3 by 37 % and 17 % for FeB and Fe_3B, and A_2 by 23 % for FeB, which means that the direction of easy axis of magnetization is ⟨1 0 0⟩ for FeB ($C_{11} < C_{22} < C_{33}$) and the hard axes directions are ⟨1 0 0⟩ and ⟨0 1 0⟩ (Fig. 6a and Fig. 6d). For Fe_3B the easy axis direction is ⟨1 0 0⟩ ($C_{11} < C_{22} < C_{33}$) and the hard axes directions are ⟨0 1 0⟩, ⟨0 0 1⟩ (Fig. 6c and Fig. 6f).

The anisotropy is only dependent on crystal symmetry. The structure of the crystal has been changed under spin polarized moment which varied a, b and c. Therefore, the elastic anisotropy is different because of the variations of the elastic constants with magnetic moment.

The elastic anisotropy of a tetragonal crystal can be measured by two shear anisotropy factors (Zener ratios) [43]:

$$A_1 = \frac{2C_{66}}{C_{11} - C_{12}} = A_2 \tag{25}$$

$$A_3 = \frac{C_{44}}{C_{11} + C_{33} - 2C_{13}} \tag{26}$$

$$(A^{\uparrow u} \cong 0)$$

Fe_2B has very low anisotropy.

The spin polarization has reduced the anisotropic factors A_1 and A_3 by 4 % and 30 % for Fe_2B, which means that the direction of easy axis of magnetization is ⟨0 0 1⟩ ($C_{33} < C_{11}$) and the directions of hard axes of magnetizations are ⟨1 0 0⟩, ⟨0 1 0⟩ (($C_{11} = C_{22}$) $> C_{33}$).

The simplest way to illustrate the anisotropy of mechanical moduli is to plot them in the three-dimensional space as a function of direction. Here, we have plotted the bulk modulus (B) and Young's modulus (E) in different directions using spherical coordinates. For orthorhombic and tetragonal crystal class, the directional dependence of bulk modulus (B) or Young's modulus (E) can be written as:

For an orthorhombic system [44]:

$$\frac{1}{B} = (S_{11} + S_{12} + S_{13})l_1^2 + (S_{12} + S_{22} + S_{23})l_2^2 + (S_{13} + S_{23} + S_{33})l_3^2 \tag{27}$$

$$\frac{1}{E} = (S_{11} + S_{22} + S_{33})l_1^4 + (2S_{12} + S_{66})l_1^2 l_2^2 + (2S_{23} + S_{44})l_2^3 l_3^2 + (2S_{13} + S_{55})l_1^2 l_3^2 \tag{28}$$

For a tetragonal system [44, 45]:

$$\frac{1}{E} = S_{11}(l_1^4 + l_1^4) + (2S_{13} + S_{44})(l_1^2 l_3^2 + l_2^2 l_3^2) + S_{33}l_3^4 + (2S_{12} + S_{66})l_1^2 l_2^2 \tag{29}$$

$$\frac{1}{B} = (S_{11} + S_{12} + S_{13})(l_1^2 l_2^2) - (2S_{13} - S_{33})l_3^2 \tag{30}$$

In the equations above, S_{ij} represents the compliance matrix and l_1, l_2 and l_3 are the direction cosines, which are given as $l_1 = \sin\theta\cos\varphi$, $l_2 = \sin\theta\sin\varphi$ and $l_3 = \cos\varphi$ in the spherical coordinates. The surface constructions of bulk and Young's modulus of FeB, Fe_2B and Fe_3B compounds are shown in Fig. 4 and Fig. 6. The surface constructions of the bulk and Young's moduli are

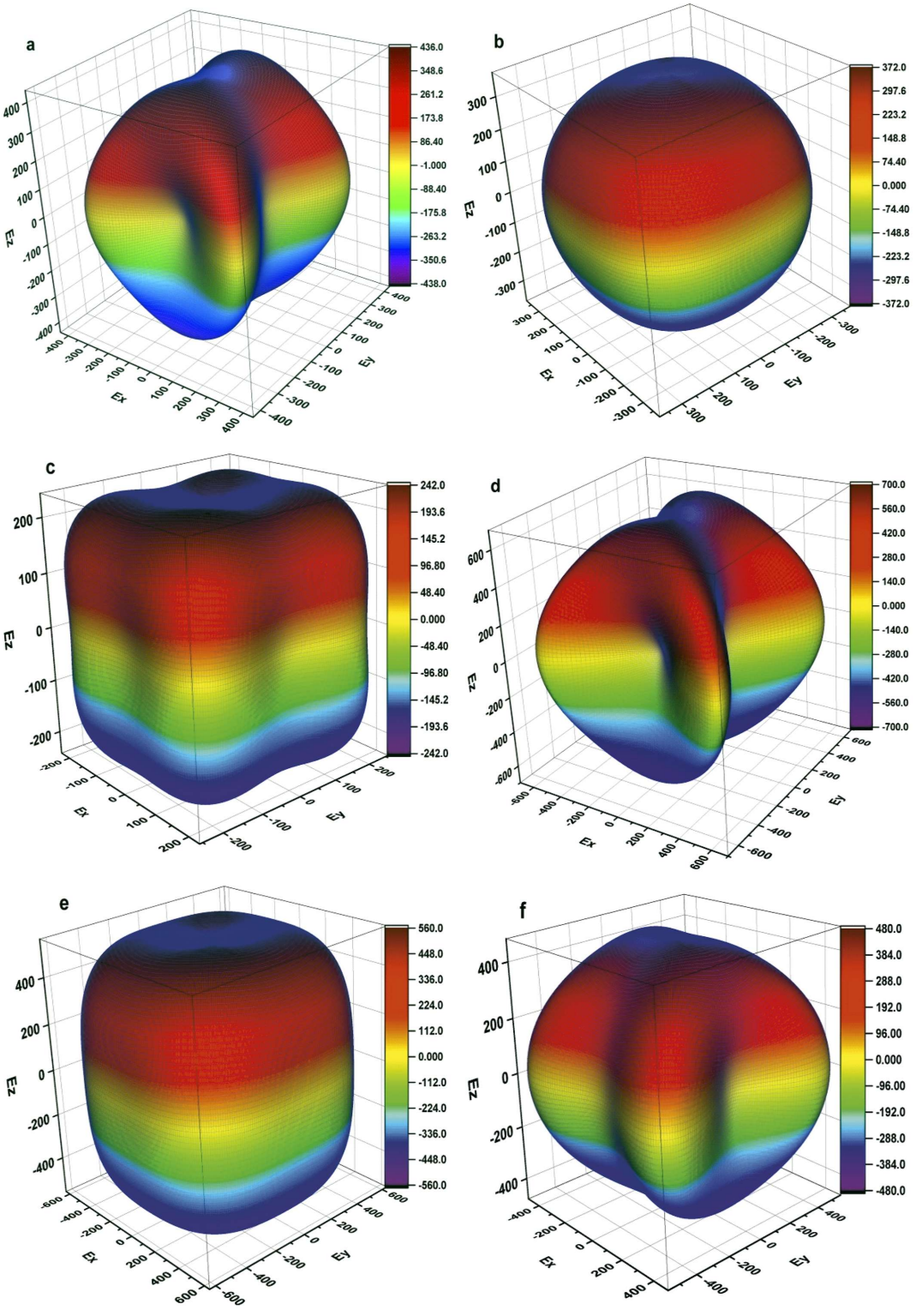

Fig. 4. Illustration of directional dependence of Young's modulus of Fe-B compounds: the left panel at 0 GPa pressure (a) FeB, (b) Fe_2B and (c) Fe3B, and the right panel at critical pressure (d) FeB 77 GPa, (e) Fe_2B 85 GPa and (f) Fe_3B 55 GPa.

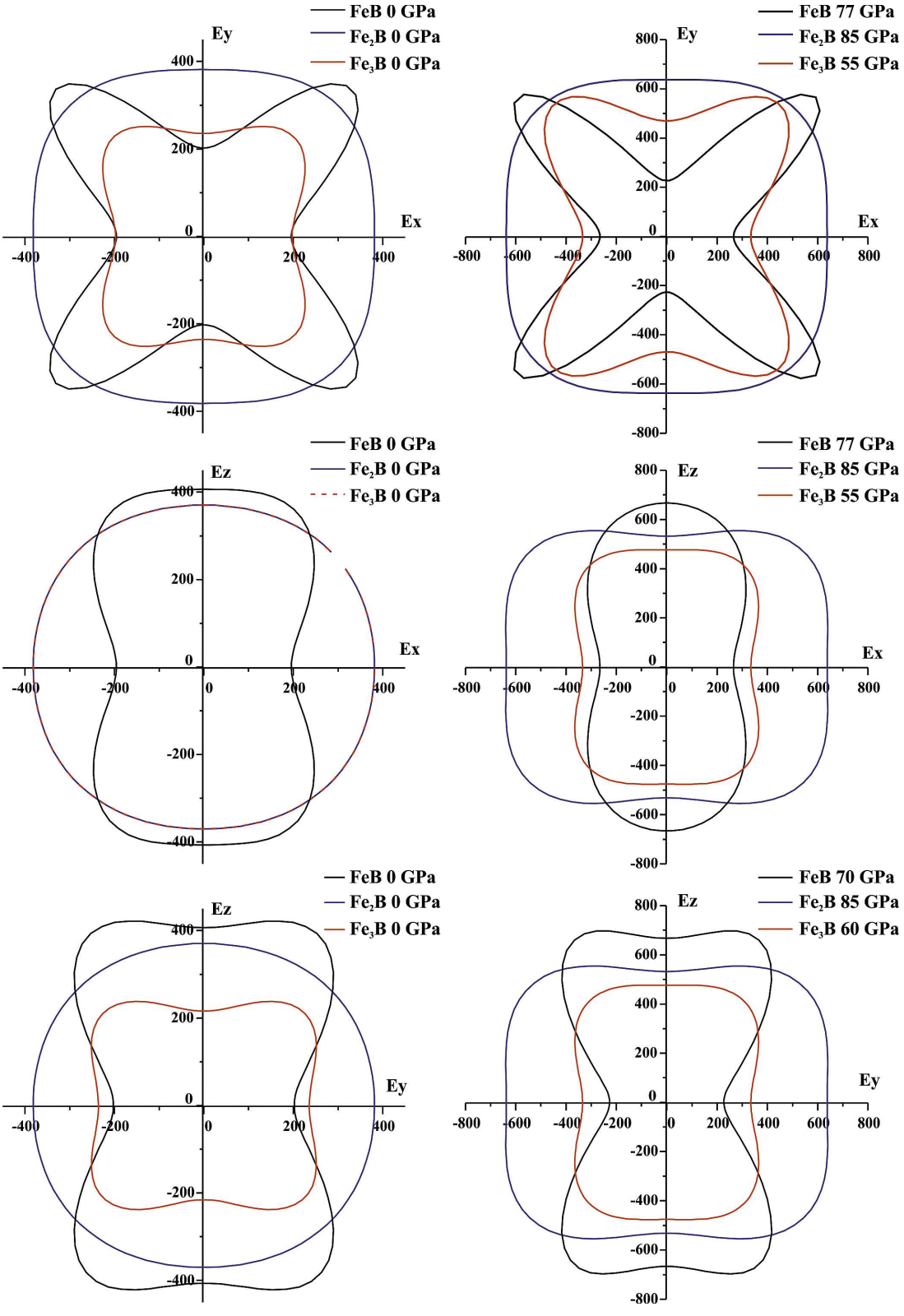

Fig. 5. Projections of Young modulus for Fe_xB compounds.

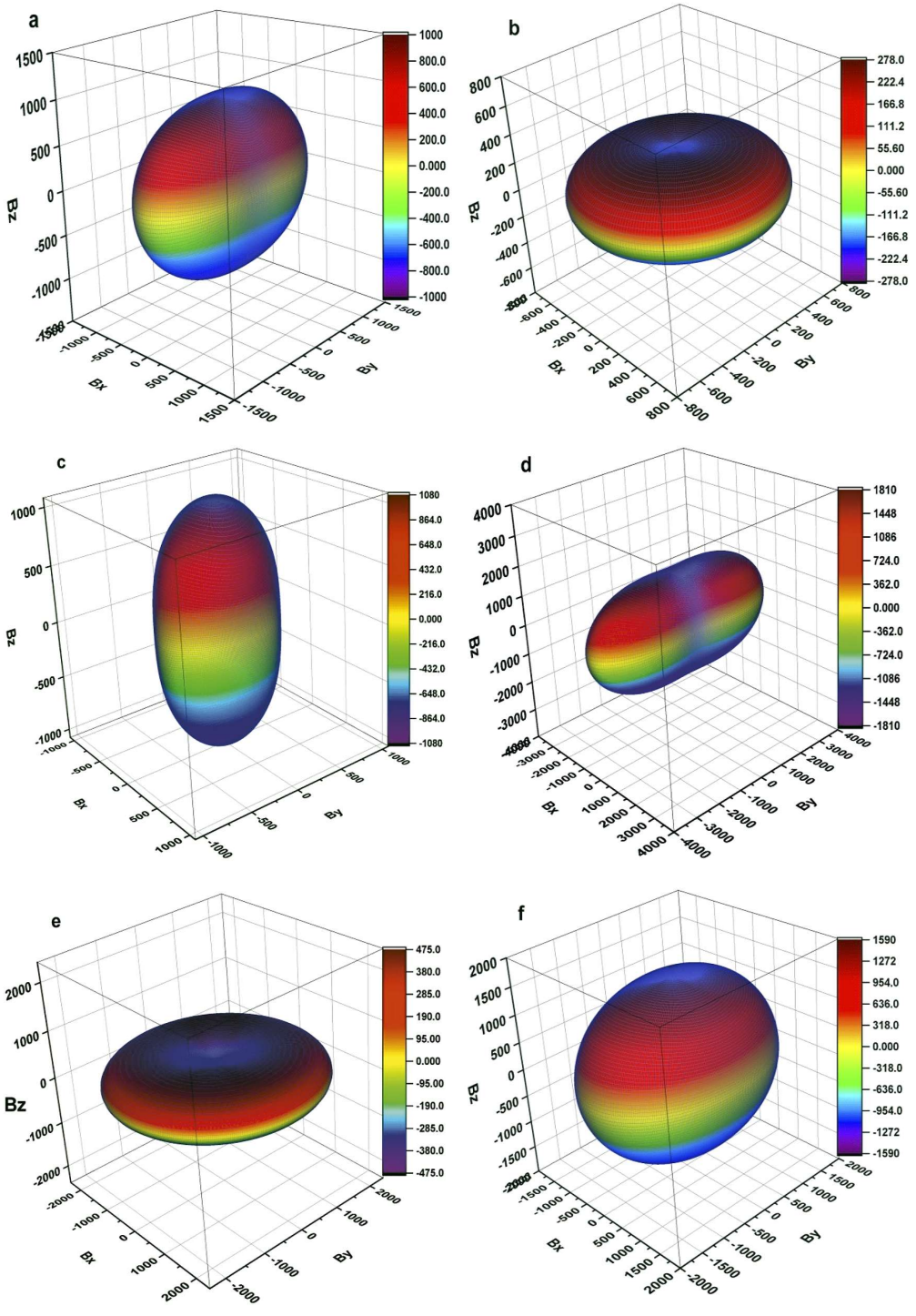

Fig. 6. Illustration of directional dependence of bulk modulus of Fe-B compounds: Left panel at 0 GPa pressure (a) FeB, (b) Fe_2B and (c) Fe_3B, and right panel at critical pressure (d) FeB 77 GPa, (e) Fe_2B 85 GPa and (f) Fe_3B 55 GPa.

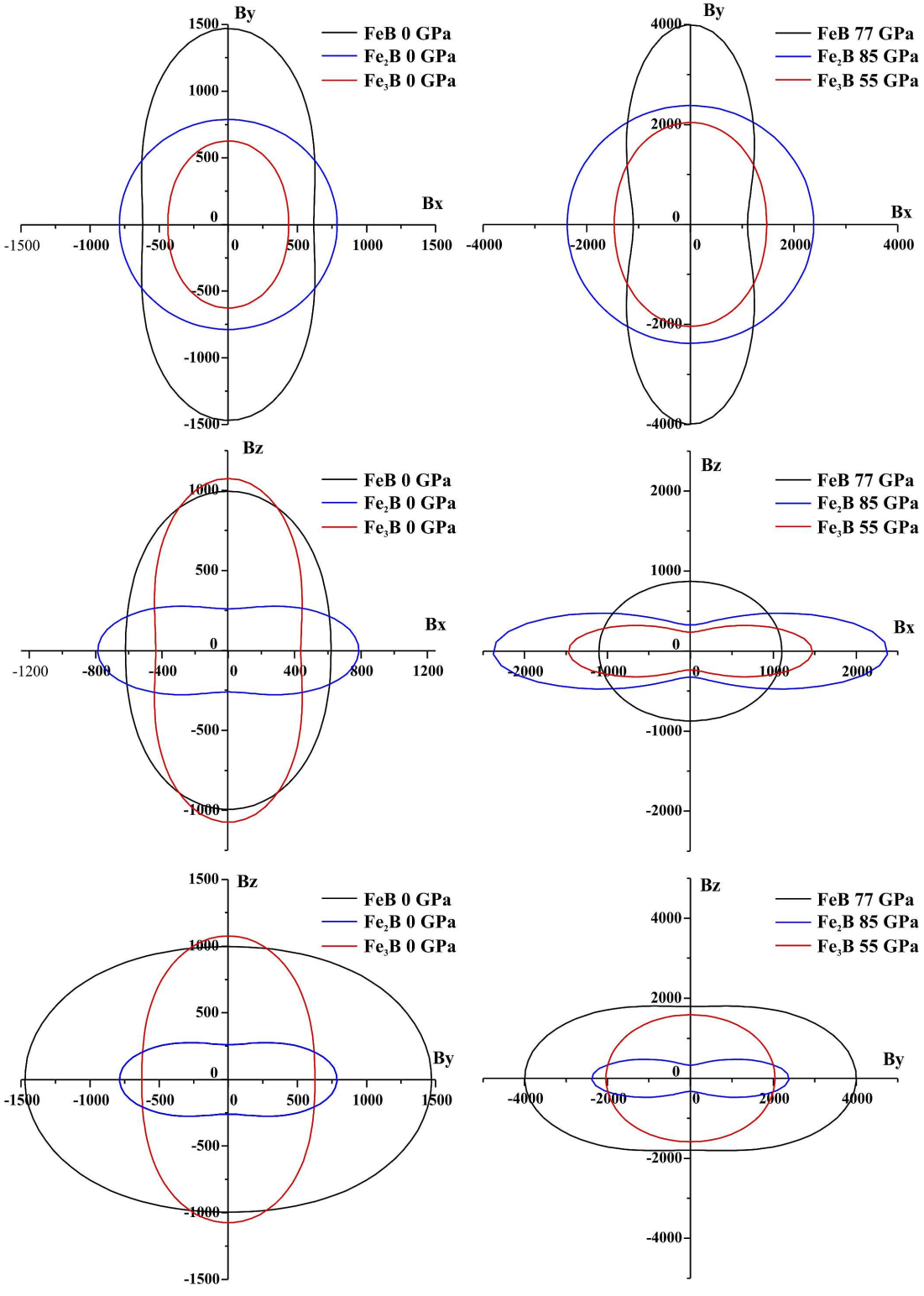

Fig. 7. Projections of bulk modulus for Fe_xB compounds.

similar to each other. The anisotropy of Young's modulus shows strong directional dependence in three crystals planes, (0 0 1), (1 0 0) and (0 1 0), for FeB structure. The projections of the mechanical moduli are plotted in Fig. 5 and Fig. 7. The results indicate that for Fe_2B the contours of bulk modulus at (0 0 1) crystal plane is spherical, implying that the bulk modulus of this phase is nearly isotropic. In the same way, the Young's modulus shows an isotropy at (0 0 1), (1 0 0) and (0 1 0) planes.

6. Conclusions

We have investigated the anisotropic elastic properties of Fe–B compounds with the help of first-principles calculations at two pressures: 0 GPa and at a critical pressure for each compound. The calculated elastic constants of all compounds clearly indicate that they are mechanically stable. Bulk modulus, shear modulus, Young's modulus and Poisson ratio have also been calculated and discussed. Disappearance of ferromagnetic order decreases the volume of the unit cell and increases the bulk modulus and also makes the solid harder. The calculated values of B/G and ν indicate that Fe_2B is ductile while FeB and Fe_3B are brittle. The degree of the elastic anisotropy for the considered Fe–B compounds follows the order $FeB > Fe_3B > Fe_2B$. We have predicted the easy and hard axes of magnetization for three compounds.

References

[1] MATUSCHKA GRAF VON A., *Boronizing*, Hanser, Philadelphia, 1980.

[2] CHATTERJEE-FISCHER R., *Boriding and Diffusion Metallizing*, in: SUDARSHAN T.S. (Ed.), *Surface Modification Technologies. An Engineer's Guide*, Marcel Dekker, New York, 1989, p. 567.

[3] GOLDSCHMIDT H.J., *Interstitial Alloys*, Springer, New York, 2013.

[4] ALLAOUI O., BOUAOUADJA N., SAINDERNAN G., *Surf. Coat. Technol.*, 201 (2006), 3475.

[5] BATTEZZATI L., ANTONIONE C., BARICCO M., *J. Alloy. Compd.*, 247 (1997), 164.

[6] HUANG Z., MA S., XING J., WANG B., *J. Alloy. Compd.*, 582 (2014), 196.

[7] ZHAO M., FENG Y., JIAO L., YUAN H., ZHOU X., JANG M.B., *Int. J. Hydrogen. Energ.*, 32 (2007), 3915.

[8] ZHANG Y.H., DONG X.P., WANG G.Q., GUO S.H., REN J.Y., WANG X.L., *T. Nonferr. Metal. Soc.*, 16 (2006), 800.

[9] ZHANG Y.H., DONG X.P., WANG G.Q., GUO S.H., REN J.Y., WANG X.L., *J. Alloy. Compd.*, 417 (2006), 224.

[10] MENESES-AMADOR A., CAMPOS-SILVA I., MARTINEZ-TRINIDAD J., PANIER S., FIGUEROA-LÓPEZ U., TORRES-HERNÁNDEZ A., *Surf. Coat. Technol.*, 215 (2013), 285.

[11] GUEDDOUH A., BENTRIA B., LEFKAIER I., *J. Magn. Magn. Mater.*, 406 (2016), 192.

[12] LU L., BANSMANN J., MEIWES-BROER K., *J. Phys. Condens. Mat.*, 10 (1998), 2873.

[13] BROWN P., COX J., *Philos. Mag.*, 23 (1971), 705.

[14] PERKINS R., BROWN P., *J. Phys. F-Metal. Phys.*, 4 (1974), 906.

[15] JOYNER D.J., JOHNSON, O., HERCULES, D. M., *J. Am. Chem. Soc.*, 102 (1980), 1910.

[16] LI G., WANG D., *J. Phys. Condens. Mat.*, 1 (1989), 1799.

[17] KOHN W., *Rev. Mod. Phys.*, 71 (1999), 1253.

[18] MEDEIROS S., ALBUQUERQUE E., MAIA F., CAETANO E., FREIRE V., *Chem. Phys. Lett.*, 435 (2007), 59.

[19] XU Y., WANG H., *J. Alloy. Compd.*, 457 (2008), 239.

[20] WANG Y., BURKE K., PERDEW, J., *Phys. Rev. B*, 54 (1996), 16533.

[21] MONKHORST H.J., PACK J.D., *Phys. Rev. B*, 13 (1976), 5188.

[22] MURPHY K.A., HERSHKOWITZ N., *Phys. Rev. B*, 7 (1973), 23.

[23] MOHN P., SCHWARZ K., MATAR S., DEMAZEAU G., *Phys. Rev. B*, 45 (1992), 4000.

[24] MOHN P., SCHWARZ K., WAGNER D., *Phys. Rev. B*, 43 (1991), 3318.

[25] DOS SANTOS A.V., KUHNEN C., *J. Solid State Chem.*, 182 (2009), 3183.

[26] CHING W., XU Y.N., HARMON B., YE J., LEUNG T., *Phys. Rev. B*, 42 (1990), 4460.

[27] BOZORT R.M., *Ferromagnetism*, Van Nostrand Company, New York, 1951, vol. 849.

[28] KITTEL C., *Introduction to solid state physics*, John Wiley & Sons, California, 2005.

[29] CHIKAZUMI S., GRAHAM C.D., *Physics of Ferromagnetism*, Oxford University Press, Oxford, 2009.

[30] EGAMI T., FINE B., SINGH D., PARSHALL D., DE LA CRUZ C., DAI P., *Physica C*, 470 (2010), S294.

[31] SHIMIZU K., KIMURA T., FUROMOTO S., TAKEDA K., KONTANI K., ONUKI Y., AMAYA K., *Nature*, 412 (2001), 316.

[32] YANG C., ZHOU Z., LI J., YANG X., QIN W., JIANG R., GUO N., WANG Y., SUN C., *Nanoscale*, 4 (2012), 1304.

[33] BECKSTEIN O., KLEPEIS J., HART G., PANKRATOV O., *Phys. Rev. B*, 63 (2001), 134112.

[34] PATIL S., KHARE S., TUTTLE B., BORDING J., KODAMBAKA S., *Phys. Rev. B*, 73 (2006), 104118.

[35] ZHOU Z., JOOS B., *Phys. Rev. B*, 54 (1996), 3841.
[36] LEWANDOWSKI J., WANG W., GREER A., *Philos. Mag. Lett.*, 85 (2005), 77.
[37] LIU Y., HU W.C., LI D.J., LI K., JIN H.L., XU Y.X., XU C.S., ZENG X.Q., *Comp. Mater. Sci.*, 97 (2015), 75.
[38] ALI K., ARYA A., GHOSH P., DEY G., *Comp. Mater. Sci.*, 112 (2016), 52.
[39] OZISIK H., COLAKOGLU K., DELIGOZ E., *Comp. Mater. Sci.*, 51 (2012), 83.
[40] RANGANATHAN S.I., OSTOJA-STARZEWSKI M., *Phys. Rev. Lett.*, 101 (2008), 055504.
[41] XIAO B., FENG J., ZHOU C., JIANG Y., ZHOU R., *J. Appl. Phys.*, 109 (2011), 023507.
[42] FENG J., XIAO B., ZHOU R., PAN W., CLARKE D.R., *Acta Mater.*, 60 (2012), 3380.
[43] GAO X., JIANG Y., ZHOU R., FENG J., *J. Alloy. Compd.*, 587 (2014), 819.
[44] DUAN Y., SUN Y., PENG M., ZHOU S., *J. Alloy. Compd.*, 595 (2014), 14.
[45] NYE J.F., *Physical Properties of Crystals: Their Representation by Tensors and Matrices*, Oxford University Press, Oxford, 1985.
[46] LI L.H., WANG W.L., HU L., WEI B.B., *Intermetallics*, 46 (2014), 211.
[47] BIALON A., HAMMERSCHMIDT T., DRAUTZ R., SHAH S., MARGINE E., KOLMOGOROV A., *Appl. Phys. Lett.*, 98 (2011), 8.

Received 2015-07-23
Accepted 2016-06-23